Adaptive Estimation of Signals of Opportunity

Zaher M. Kassas and Vaibhav Ghadiok
The University of California, Riverside
Todd E. Humphreys
The University of Texas at Austin

BIOGRAPHIES

Zaher (Zak) M. Kassas is an assistant professor at The University of California, Riverside. He received a B.E. in Electrical Engineering from The Lebanese American University, an M.S. in Electrical and Computer Engineering from The Ohio State University, and an M.S.E. in Aerospace Engineering and a Ph.D. in Electrical and Computer Engineering from The University of Texas at Austin. From 2004 through 2010 he was a research and development engineer with the LabVIEW Control Design and Dynamical Systems Simulation Group at National Instruments Corp. His research interests include estimation, navigation, autonomous vehicles, and intelligent transportation systems.

Vaibhav Ghadiok is a Ph.D. candidate in the Department of Electrical and Computer Engineering at The University of California, Riverside. He received a B.S. in Electronics and Instrumentation Engineering from R.V. College of Engineering, India, and an M.S. in Electrical Engineering from Utah State University. His research interests are in vision- and RF-based navigation and control of distributed multi-agent systems.

Todd E. Humphreys is an assistant professor in the Department of Aerospace Engineering and Engineering Mechanics at The University of Texas at Austin, and Director of The University of Texas Radionavigation Laboratory. He received a B.S. and an M.S. in Electrical and Computer Engineering from Utah State University and a Ph.D. in Aerospace Engineering from Cornell University. He specializes in applying optimal estimation and signal processing techniques to problems in radionavigation. His recent focus is on radionavigation robustness and security.

ABSTRACT

To exploit unknown ambient radio frequency signals of opportunity (SOPs) for positioning and navigation, one must estimate their states along with a set of parameters that characterize the stability of their oscillators. SOPs can be modeled as stochastic dynamical systems driven by process noise. The statistics of such process noise is typically unknown to the receiver wanting to exploit the SOPs for positioning and navigation. Incorrect statistical models jeopardize the estimation optimality and may cause filter divergence. This necessitates the development of adaptive filters, which provide a significant improvement over fixed filters through the filter learning process. This paper develops two such adaptive filters: an innovation-based maximum likelihood filter and an interacting multiple model filter and compares their performance and complexity. Numerical and experimental results are presented demonstrating the superiority of these filters over fixed, mismatched filters.

I. INTRODUCTION

The plenitude of ambient radio frequency signals in Global Navigation Satellite System (GNSS)-challenged environments make them an attractive choice for exploitation for positioning and navigation [1–3]. These signals are commonly referred to as signals of opportunity (SOPs) and include cellular phone signals [4, 5], television signals [6], AM/FM radio signals [7], WiFi signals [8], Iridium satellite signals [9, 10], XM$^{\text{TM}}$ satellite signals [11], and light-emitting diode (LED) signals [12], among others.

To exploit an SOP for positioning and navigation, one must estimate the SOP's states, namely, the position and velocity of the SOP transmitter's antenna phase center, the SOP's time offset from a reference time base, and rate of change of time offset, along with a set of parameters that characterize the SOP's reference oscillator stability. An SOP can be modeled as a stochastic dynamical system driven by process noise, where the statistics of such process noise is a function of the SOP's oscillator stability. Such statistics can be related to the so-called h-parameters, which characterize the spectra of the fractional frequency deviation of oscillators.

The observability of environments comprising multiple receivers with velocity random walk dynamics making pseudorange observations on multiple SOPs was thoroughly analyzed in [13] and the states' estimability was assessed in [14]. Motion planning for optimal simultaneous receiver localization and signal landscape mapping of environments comprising multiple SOPs was addressed in [15–19]. However, all such work assumed knowledge of the statistical models of the process and observation noise.

A receiver entering a new signal landscape cannot assume the availability of high-fidelity statistical models describing the SOPs. Incorrect models jeopardize the estimation optimality and may cause filter divergence. Hence, the receiver's estimator need to: (i) perform on-the-fly sig-

Preprint of the 2014 ION GNSS+ Conference
Tampa, FL, September 8–12, 2014

nal characterization for discovered SOPs and (*ii*) continuously refine estimates of SOPs' parameters of relevance. Therefore, adaptive estimators, which provide a significant improvement over fixed filters through the filter learning process, will be necessary.

The main application of adaptive filters in navigation systems have been in coupling inertial navigation systems (INS) with GNSS receivers [20–23]. Adaptive filters can be classified into those that estimate the estimation error covariances directly and those that explicitly estimate the process and observation noise covariances. While the former methods could suffice for single receivers, the latter techniques are more suitable for multiple collaborating receivers whose objective is to share information intrinsic to the SOPs through a signal characterization database [1,2].

Navigation tracking loops could estimate the observation noise variances associated with pseudorange and carrier phase observations through explicit relationships relating the tracking loop characteristics to the carrier-to-noise ratio C/N_0 [24]. However, estimating the process noise covariance describing the stability of the SOP's oscillator is not as straightforward. This is the subject of this paper. To this end, adaptive filters that estimate the process noise covariances pertaining to the SOP clock error states (i.e., bias and drift) will be designed. The objective of these filters is twofold: (*i*) improve the estimates of the SOP states and (*ii*) produce estimates of the statistical model governing the SOP's oscillator stability, which can be shared with other receivers through a signal characterization database.

Off-line techniques to estimate the h-parameters via spectral methods exist [25,26]. However, to our knowledge, estimating the statistics of the clock error states in an adaptive estimation framework has not been addressed before. This paper's contribution is to design appropriate adaptive filters for receivers making pseudorange observations on unknown SOPs. To this end, two adaptive filters will be studied: a simple maximum-likelihood (ML) adaptive Kalman filter (KF) and a more involved interacting multiple model (IMM) filter. Numerical simulation and experimental results for single and multiple receivers will be presented comparing the two adaptive filters and demonstrating their superiority over fixed, mismatched filters.

The remainder of this paper is organized as follows. Section II describes the clocks, receiver, and SOP dynamical models and the pseudorange observation model. Section III gives a brief overview of the different classes of adaptive filters and summarizes the computations involved in the ML and IMM. Section IV presents simulation results comparing the performance of matched, mismatched, and adaptive filters. Section V presents experimental results illustrating the application of the various filters into estimating the states and process noise statistics of an unknown cellular SOP. Concluding remarks are given in Section VI.

II. MODEL DESCRIPTION

A. Clock Dynamics Model

The receiver and SOP clock error dynamics will be modeled according to the two-state model composed of the clock bias δt and clock drift $\dot{\delta t}$, as depicted in Fig. 1. The clock error states evolve according to

$$\dot{\boldsymbol{x}}_{\text{clk}}(t) = \mathbf{A}_{\text{clk}}\, \boldsymbol{x}_{\text{clk}}(t) + \tilde{\boldsymbol{w}}_{\text{clk}}(t),$$

$$\boldsymbol{x}_{\text{clk}} = \begin{bmatrix} \delta t \\ \dot{\delta t} \end{bmatrix}, \quad \tilde{\boldsymbol{w}}_{\text{clk}} = \begin{bmatrix} \tilde{w}_{\delta t} \\ \tilde{w}_{\dot{\delta t}} \end{bmatrix}, \quad \mathbf{A}_{\text{clk}} = \begin{bmatrix} 0 & 1 \\ 0 & 0 \end{bmatrix},$$

where the elements of $\tilde{\boldsymbol{w}}_{\text{clk}}$ are modeled as zero-mean, mutually independent white noise processes and the power spectral density of $\tilde{\boldsymbol{w}}_{\text{clk}}$ is given by $\tilde{\mathbf{Q}}_{\text{clk}} = \text{diag}\left[S_{\tilde{w}_{\delta t}}, S_{\tilde{w}_{\dot{\delta t}}}\right]$. The power spectra $S_{\tilde{w}_{\delta t}}$ and $S_{\tilde{w}_{\dot{\delta t}}}$ can be related to the power-law coefficients $\{h_\alpha\}_{\alpha=-2}^{2}$, which have been shown through laboratory experiments to be adequate to characterize the power spectral density of the fractional frequency deviation $y(t)$ of an oscillator from nominal frequency, which takes the form $S_y(f) = \sum_{\alpha=-2}^{2} h_\alpha f^\alpha$ [27,28]. It is common to approximate the clock error dynamics by considering only the frequency random walk coefficient h_{-2} and the white frequency coefficient h_0, which lead to $S_{\tilde{w}_{\delta t}} \approx \frac{h_0}{2}$ and $S_{\tilde{w}_{\dot{\delta t}}} \approx 2\pi^2 h_{-2}$ [29,30].

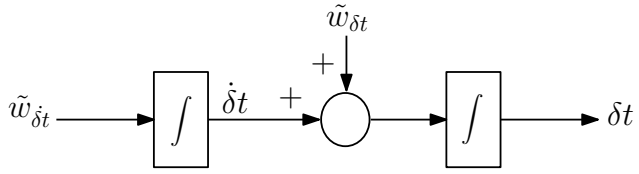

Fig. 1. Clock error states dynamical model

B. Receiver Dynamics Model

The receiver's position $\boldsymbol{r}_r$ and velocity $\dot{\boldsymbol{r}}_r$ will be assumed to evolve according to a velocity random walk model given by

$$\dot{\boldsymbol{x}}_{\text{pv}}(t) = \mathbf{A}_{\text{pv}}\, \boldsymbol{x}_{\text{pv}}(t) + \mathbf{D}_{\text{pv}} \tilde{\boldsymbol{w}}_{\text{pv}}(t),$$

$$\mathbf{A}_{\text{pv}} = \begin{bmatrix} \mathbf{0}_{2\times 2} & \mathbf{I}_{2\times 2} \\ \mathbf{0}_{2\times 2} & \mathbf{0}_{2\times 2} \end{bmatrix}, \quad \mathbf{D}_r = \begin{bmatrix} \mathbf{0}_{2\times 2} \\ \mathbf{I}_{2\times 2} \end{bmatrix}$$

$$\boldsymbol{x}_{\text{pv}} = \begin{bmatrix} \boldsymbol{r}_r^{\mathsf{T}} & \dot{\boldsymbol{r}}_r^{\mathsf{T}} \end{bmatrix}^{\mathsf{T}}, \; \boldsymbol{r}_r = \begin{bmatrix} x_r & y_r \end{bmatrix}^{\mathsf{T}}, \; \tilde{\boldsymbol{w}}_{\text{pv}} = \begin{bmatrix} \tilde{w}_x & \tilde{w}_y \end{bmatrix}^{\mathsf{T}},$$

where the elements of $\tilde{\boldsymbol{w}}_{\text{pv}}$ are modeled as zero-mean, mutually-independent, white noise processes with power spectral densities $\tilde{q}_x$ and $\tilde{q}_y$, respectively.

The receiver's state vector $\boldsymbol{x}_r$ is defined by augmenting the receiver's position and velocity with its clock error states,

i.e., $\boldsymbol{x}_r \triangleq \left[\boldsymbol{x}_{\text{pv}}^{\mathsf{T}},\, \boldsymbol{x}_{\text{clk,r}}^{\mathsf{T}}\right]^{\mathsf{T}}$. Discretizing the receiver's dynamics at a constant sampling period T yields the discrete-time (DT) model

$$\boldsymbol{x}_r\,(k+1) = \mathbf{F}_r\,\boldsymbol{x}_r(k) + \boldsymbol{w}_r(k), \quad k = 0, 1, 2, \ldots$$

where $\boldsymbol{w}_r$ is a DT zero-mean white noise sequence with covariance $\mathbf{Q}_r = \text{diag}\,[\mathbf{Q}_{\text{pv}},\, \mathbf{Q}_{\text{clk},r}]$, with

$$\mathbf{F}_r = \begin{bmatrix} \mathbf{I}_{2\times2} & T\mathbf{I}_{2\times2} & \mathbf{0}_{2\times2} \\ \mathbf{0}_{2\times2} & \mathbf{I}_{2\times2} & \mathbf{0}_{2\times2} \\ \mathbf{0}_{2\times2} & \mathbf{0}_{2\times2} & \mathbf{F}_{\text{clk}} \end{bmatrix}, \quad \mathbf{F}_{\text{clk}} = \begin{bmatrix} 1 & T \\ 0 & 1 \end{bmatrix}$$

$$\mathbf{Q}_{\text{clk},r} = \begin{bmatrix} S_{\tilde{w}_{\delta t_r}} T + S_{\tilde{w}_{\dot{\delta} t_r}} \frac{T^3}{3} & S_{\tilde{w}_{\dot{\delta} t_r}} \frac{T^2}{2} \\ S_{\tilde{w}_{\dot{\delta} t_r}} \frac{T^2}{2} & S_{\tilde{w}_{\delta t_r}} T \end{bmatrix}$$

$$\mathbf{Q}_{\text{pv}} = \begin{bmatrix} \tilde{q}_x \frac{T^3}{3} & 0 & \tilde{q}_x \frac{T^2}{2} & 0 \\ 0 & \tilde{q}_y \frac{T^3}{3} & 0 & \tilde{q}_y \frac{T^2}{2} \\ \tilde{q}_x \frac{T^2}{2} & 0 & \tilde{q}_x T & 0 \\ 0 & \tilde{q}_y \frac{T^2}{2} & 0 & \tilde{q}_y T \end{bmatrix}.$$

C. SOP Dynamics Model

The SOP will be assumed to emanate from a spatially-stationary terrestrial transmitter, and its state will consist of its planar position and clock error states. Hence, the SOP's dynamics can be described by the state space model

$$\dot{\boldsymbol{x}}_s(t) = \mathbf{A}_s\,\boldsymbol{x}_s(t) + \mathbf{D}_s \tilde{\boldsymbol{w}}_s(t), \tag{1}$$

where $\boldsymbol{x}_s = \left[\boldsymbol{r}_s^{\mathsf{T}},\, \boldsymbol{x}_{\text{clk,s}}^{\mathsf{T}}\right]^{\mathsf{T}}$, $\boldsymbol{r}_s = [x_s,\, y_s]^{\mathsf{T}}$, $\tilde{\boldsymbol{w}}_s = \left[\tilde{w}_{\delta t_s},\, \tilde{w}_{\dot{\delta} t_s}\right]^{\mathsf{T}}$

$$\mathbf{A}_s = \begin{bmatrix} \mathbf{0}_{2\times2} & \mathbf{0}_{2\times2} \\ \mathbf{0}_{2\times2} & \mathbf{A}_{\text{clk}} \end{bmatrix}, \quad \mathbf{D}_s = \begin{bmatrix} \mathbf{0}_{2\times2} \\ \mathbf{I}_{2\times2} \end{bmatrix}.$$

Discretizing the SOP's dynamics (1) at a sampling interval T yields the DT-equivalent model

$$\boldsymbol{x}_s\,(k+1) = \mathbf{F}_s\,\boldsymbol{x}_s(k) + \boldsymbol{w}_s(k),$$

where $\boldsymbol{w}_s$ is a DT zero-mean white noise sequence with covariance $\mathbf{Q}_s$, and

$$\mathbf{F}_s = \text{diag}\,[\mathbf{I}_{2\times2},\, \mathbf{F}_{\text{clk}}], \quad \mathbf{Q}_s = \text{diag}\,[\mathbf{0}_{2\times2},\, \mathbf{Q}_{\text{clk},s}],$$

where $\mathbf{Q}_{\text{clk},s}$ is identical to $\mathbf{Q}_{\text{clk},r}$, except that $S_{\tilde{w}_{\delta t_r}}$ and $S_{\tilde{w}_{\dot{\delta} t_r}}$ are now replaced with SOP-specific spectra, $S_{\tilde{w}_{\delta t_s}}$ and $S_{\tilde{w}_{\dot{\delta} t_s}}$, respectively.

D. Observation Model

The pseudorange observation made by the receiver on the SOP, after discretization and mild approximations discussed in [13], is given by

$$z(k) = \|\boldsymbol{r}_r(k) - \boldsymbol{r}_s(k)\|_2 + c\cdot[\delta t_r(k) - \delta t_s(k)] + v_\rho(k), \tag{2}$$

where c is the speed of light and v_ρ is a DT zero-mean white Gaussian sequence with variance r.

III. OVERVIEW OF ADAPTIVE FILTERS

Adaptive estimation approaches can be categorized into Bayesian, covariance matching, correlation, maximum likelihood (ML), and hybrid methods. Bayesian techniques suffer from the curse of dimensionality and assume stationarity of the process noise [31, 32]. Covariance matching techniques rely on the principle of making the time average of squared innovations consistent with the ensemble average; hence, they implicitly assume ergodicity of the noise. Tuning the process noise covariance is typically done in an ad-hoc manner, making the convergence of these techniques questionable [31,33]. Correlation methods assume ergodicity of the noise and rely on establishing relationships between the noise statistics and the autocorrelation of the measurement or residual sequences. They have been shown to be a fruitful approach [31, 34, 35]. In ML techniques, the likelihood function is maximized to obtain estimates of the noise statistics, and the chain rule of probability distributions is typically invoked. A unique solution is only guaranteed whenever the dimension of the observation vector is greater than or equal to the dimension of the state vector [31, 36, 37]. The most popular hybrid techniques are the multiple-model adaptive estimator (MMAE) [38] and the interacting multiple-model (IMM) estimator [39]. Both maintain a bank of KFs matched to the various modes at which the system may be operating. The innovation likelihoods from each filter are used to weight the filter estimates to form a combined state estimate. The MMAE directly uses these likelihoods as adaptive weights, which could cause the filter to get "stuck" onto a particular mode. To rectify this behavior, minimum threshold probabilities are typically assigned to each filter. The IMM circumvents this problem with the introduction of an interaction/mixing step in which state estimates given to the bank of filters are calculated at each time step using the weighted estimates of the previous time step.

The next two subsections summarize the main computations involved in two candidate adaptive filters, which this paper study: the simple ML-based adaptive KF and the more involved IMM filter.

A. MAXIMUM LIKELIHOOD ADAPTIVE KALMAN FILTER

In ML-based adaptive Kalman filtering, the process noise covariance matrix $\mathbf{Q}$ is estimated using either the innovation $\boldsymbol{\nu}$ or state correction $\Delta\boldsymbol{x}$. This estimate is subsequently fed-back within a Kalman filtering framework [20, 40]. The innovation is defined as

$$\boldsymbol{\nu}(k+1) \triangleq \boldsymbol{z}(k+1) - \hat{\boldsymbol{z}}(k+1|k),$$

where $\boldsymbol{z}(k+1)$ is the measurement and $\hat{\boldsymbol{z}}(k+1|k)$ is the predicted measurement. The state correction is defined as

$$\Delta\boldsymbol{x}(k+1) \triangleq \hat{\boldsymbol{x}}(k+1|k+1) - \hat{\boldsymbol{x}}(k+1|k),$$

where $\hat{\boldsymbol{x}}(k+1|k+1)$ is the updated state estimate and $\hat{\boldsymbol{x}}(k+1|k)$ is the predicted state estimate.

The estimate of process noise covariance $\hat{\mathbf{Q}}$ using $\Delta\boldsymbol{x}$ is computed as

$$\hat{\mathbf{Q}}(k+1) \triangleq \frac{1}{N}\sum_{j=k-N+2}^{k+1}\Delta\boldsymbol{x}(j)\Delta\boldsymbol{x}^{\mathsf{T}}(j) + \mathbf{P}(k+1|k+1) - \mathbf{F}\mathbf{P}(k|k)\mathbf{F}^{\mathsf{T}}, \quad (3)$$

where $\mathbf{P}$ is the estimation error covariance, $\mathbf{F}$ is the state transition matrix, and $\frac{1}{N}\sum_{j=k-N+2}^{k+1}\Delta\boldsymbol{x}(j)\Delta\boldsymbol{x}^{\mathsf{T}}(j)$ is the covariance of the state corrections, averaged over a sliding window of length N. The first estimate of $\mathbf{Q}$ is obtained after N time steps and is subsequently fed-back to the KF. In practice, additional constraints of positive-definiteness need to be enforced for $\hat{\mathbf{Q}}$. This may be achieved by dropping the last two terms in (3) [21, 41].

When the filter is in steady-state, (3) can be approximated by

$$\hat{\mathbf{Q}}(k+1) \approx \mathbf{W}(k+1)\mathbf{C}_{\nu}(k+1)\mathbf{W}^{\mathsf{T}}(k+1),$$

where $\mathbf{C}_{\nu}(k+1)$ is an estimate of the innovation covariance that is obtained by averaging the previous innovation sequence over a window of length N, namely $\mathbf{C}_{\nu}(k+1) \triangleq \frac{1}{N}\sum_{j=k-N+2}^{k+1}\boldsymbol{\nu}(j)\boldsymbol{\nu}^{\mathsf{T}}(j)$, and $\mathbf{W}$ is the Kalman gain [41].

Note that the above formulation implicitly assumes that the system is observable, the innovation sequence is white and ergodic, and the measurement noise covariance matrix $\mathbf{R}$ is completely known.

This adaptive estimation scheme is attractive due to: (i) relying on ML, which provides uniqueness and consistency of the estimates and (ii) involving simple computations. However, the window size N needs to be tuned to trade-off adaptability versus stability of the filter.

B. INTERACTING MULTIPLE MODEL ADAPTIVE ESTIMATION

In multiple model (MM) estimation, the system is assumed to obey one of a finite number of modes, and a bank of estimators (usually KFs) run in parallel, where each filter is matched to a particular mode. A state estimate is computed by summing the individual filter estimates, weighted by their respective innovation likelihoods [29].

An optimal estimator would keep a track of the entire history of mode changes; however, this makes the estimation problem exponentially hard. Therefore, sub-optimal techniques are typically employed. Two solutions are the generalized pseudo-Bayesian (GPB) algorithms, known as GPB1 and GPB2, which store one time step (r hypotheses) and two time steps (r^2 hypotheses), respectively, where r is the number of modes [29].

To balance computational efficiency and accuracy of the solution, the IMM filter was proposed [29, 42]. In IMM, the input to each filter is given as a weighted combination of the estimates of the filters at the previous time step. This step, called the interaction/mixing step, is able to approximately encapsulate information from the last two time steps using only r filters, as compared to r^2 filters in GPB2.

A single cycle of the IMM for $r = 2$ is depicted in Fig. 2, with the following notational definitions:

r	Number of filters
i	$\{1, \ldots, r\} \in \mathbb{N}$
$\hat{\boldsymbol{x}}^{i}(k\|k)$	State estimate of filter i
$\mathbf{P}^{i}(k\|k)$	Estimation error covariance of filter i
$\boldsymbol{\mu}(k\|k)$	Mixing probability matrix
$\hat{\boldsymbol{x}}^{0i}(k\|k)$	Mixed initial condition matched to filter i
$\mathbf{P}^{0i}(k\|k)$	Estimation error covariance associated with $\hat{\boldsymbol{x}}^{0i}(k\|k)$
$\boldsymbol{z}(k+1)$	Measurement
$\Lambda_i(k+1)$	Innovation likelihood of of filter i
$\hat{\boldsymbol{x}}^{i}(k+1\|k+1)$	Updated state estimate of filter i
$\mathbf{P}^{i}(k+1\|k+1)$	Updated estimation error covariance of filter i
$\boldsymbol{\mu}(k+1)$	Mode probability vector
$\hat{\boldsymbol{x}}(k+1\|k+1)$	Combined state estimate
$\mathbf{P}(k+1\|k+1)$	Combined estimation error covariance

The IMM consists of four stages: interaction/mixing, filtering, mode update, and combination, which are summarized next.

Interaction/Mixing This stage calculates $\hat{\boldsymbol{x}}^{0i}(k|k)$ and $\mathbf{P}^{0i}(k|k)$ by combining $\hat{\boldsymbol{x}}^{i}(k|k)$ and $\mathbf{P}^{i}(k|k)$ through weighting their corresponding mixing probabilities from $\boldsymbol{\mu}(k|k)$.

Filtering This stages performs a regular KF update (prediction and correction), for each KF in the bank, where each filter is matched to a particular mode. It also calculates the innovation likelihood functions.

Mode and mixing probability update This stage updates the mode probability vector and mixing probability matrix, based on the innovation likelihoods.

State estimate and covariance combination This stage combines the state estimates and estimation error covariances from the individual filters by weighting

$\hat{\boldsymbol{x}}^i(k+1|k+1)$ and $\mathbf{P}^i(k+1|k+1)$ by their respective mode probabilities from $\boldsymbol{\mu}(k+1)$.

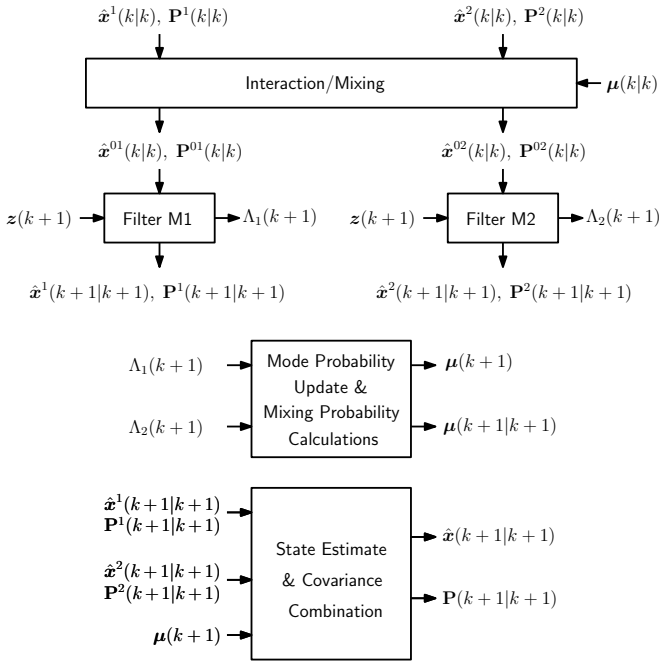

Fig. 2. Single cycle of the IMM filter for $r = 2$

Generally, each mode in the IMM is initialized with a different $\hat{\boldsymbol{x}}^i$, $\mathbf{P}^i$, $\mathbf{Q}^i$, and $\mathbf{R}^i$. A mode transition probability matrix $\boldsymbol{\pi}$ is specified to model the Markov chain transition probabilities between the different modes.

The IMM was extended to estimating the unknown process noise statistics in [39], where a bank of two KFs is identically initialized with the exception of $\mathbf{Q}^i$. One of the filters is initialized with an upper-bound $\mathbf{Q}_{\max}$, while the other is initialized with a lower-bound $\mathbf{Q}_{\min}$, corresponding to the worst and best case process noise scenarios. In this scheme, the noise covariance estimate $\hat{\mathbf{Q}}$ is computed as

$$\hat{\mathbf{Q}}(k+1) = \sum_{i=1}^{2} \boldsymbol{\mu}_i(k+1)\, \mathbf{Q}^i(k+1). \tag{4}$$

A numerically better estimate for $\hat{\mathbf{Q}}$ can be achieved using the matrix square root as

$$\begin{aligned} \hat{\mathbf{Q}}^{1/2}(k+1) &= \sum_{i=1}^{2} \boldsymbol{\mu}_i(k+1) \left[\mathbf{Q}^i(k+1)\right]^{1/2} \\ \hat{\mathbf{Q}}_{\mathrm{SD}}(k+1) &= \hat{\mathbf{Q}}^{1/2}(k+1)\hat{\mathbf{Q}}^{1/2}(k+1) \end{aligned} \tag{5}$$

The IMM is attractive due to the following reasons: (i) it has a fixed computational cost per cycle, (ii) it can be applied to systems with non-stationary noise and rapidly varying statistics, and (iii) it is self-tuning.

IV. SIMULATION RESULTS

This section presents simulation results demonstrating the application of ML and IMM adaptive filters. Subsection IV-A considers the case of a single receiver estimating the states and process noise covariance of one unknown SOP, while Subsection IV-B tackles the case of collaborative estimation of the states and process noise covariance of one unknown SOP via multiple receivers.

A. Single Receiver

A.1 Simulations Setup

Consider an environment with a single receiver with perfect knowledge about its own states (through having access to GNSS observables, for example) and moving according to the velocity random walk dynamics described in Subsection II-B. This receiver makes pseudorange observations on an unknown SOP according to (2). It was shown in [13] that such scenario is fully-observable.

Three sets of simulations are performed, each assuming a different truth model for the SOP, specifically an SOP with (i) the best oven-controlled crystal oscillator (OCXO), (ii) a typical OCXO, and (iii) the worst temperature-compensated crystal oscillator (TCXO). The simulation settings are given in Table I, where $v_{\max}$ is the maximum speed with which the receiver can move, and the h-parameters values were obtained from [43]. For purposes of numerical stability, the clock error states were defined as $c\delta t$ and $c\dot{\delta}t$.

Three sets of filters are developed and compared:

Matched An extended Kalman filter (EKF) that is initialized with the true $\mathbf{Q}$ will serve as a reference for the optimal achievable performance whenever the process noise covariance is perfectly known

Mismatched A number of mismatched, fixed EKFs, each initialized with a different $\mathbf{Q}$, will demonstrate the performance of the filter if one chooses to fix $\mathbf{Q}$ to some "typical" value without adaptation

Adaptive The ML and IMM adaptive filters will demonstrate the achieved performance whenever the filter is simultaneously estimating $\boldsymbol{x}_s$ while adapting $\mathbf{Q}$

For the sake of meaningful comparison, each estimator is initialized with the same initial estimate $\hat{\boldsymbol{x}}_s$, and the same process and observation noise realization per simulation run is used. The IMM used a bank of two EKFs with $\left\{\mathbf{Q}^i\right\}_{i=1}^2$ corresponding to the best OCXO and worst TCXO, respectively. The initial mode probability and mode transition probabilities were set at

$$\boldsymbol{\mu} \begin{bmatrix} 0.5 \\ 0.5 \end{bmatrix}, \quad \boldsymbol{\pi} = \begin{bmatrix} 0.999 & 0.001 \\ 0.001 & 0.999 \end{bmatrix},$$

which indicates our lack of *a priori* knowledge about whether the SOP is an OCXO or a TCXO, and our assertion that the process noise is not likely to switch modes. The ML filter was initialized assuming an average clock, i.e., with an initial process noise covariance of $\mathbf{Q}_{\text{avg}} = (\mathbf{Q}_1 + \mathbf{Q}_2)/2$, which also indicates our lack of *a priori* knowledge about whether the SOP is an OCXO or a TCXO. The total simulation time was 400s and a sample receiver trajectory is shown in Fig. 3. Single-run and Monte Carlo (MC) simulation results over 100 runs for each case are presented next.

TABLE I
SIMULATION SETTINGS

Parameter	**Value**
$\boldsymbol{x}_r(0)$	$[400,\ 400,\ 0,\ 0,\ 10,\ 1]^{\mathsf{T}}$
$\boldsymbol{x}_s(0)$	$[50,\ 100,\ 1,\ 0.1]^{\mathsf{T}}$
$\hat{\boldsymbol{x}}_s(0\vert-1)$	$\sim \mathcal{N}[\boldsymbol{x}_s(0), \mathbf{P}_s(0\vert-1)]$
$\mathbf{P}_s(0\vert-1)$	$(10^3)\cdot \text{diag}\,[1, 1, 30, 0.3]$
Best OCXO $\{h_{0,\text{s}},\ h_{-2,\text{s}}\}$	$\{2.6\times10^{-22},\ 4.0\times10^{-26}\}$
Worst TCXO $\{h_{0,\text{s}},\ h_{-2,\text{s}}\}$	$\{2.0\times10^{-19},\ 2.0\times10^{-20}\}$
Typical OCXO $\{h_{0,\text{s}},\ h_{-2,\text{s}}\}$	$\{8.0\times10^{-20},\ 4.0\times10^{-23}\}$
Typical TCXO $\{h_{0,\text{s}},\ h_{-2,\text{s}}\}$	$\{9.4\times10^{-20},\ 3.8\times10^{-21}\}$
$\tilde{q}_x, \tilde{q}_y$	$0.5\,(\text{m/s}^2)^2$
r	$40\,\text{m}^2$
$v_{\max}$	$10\,\text{m/s}$
T	$0.1\,\text{s}$

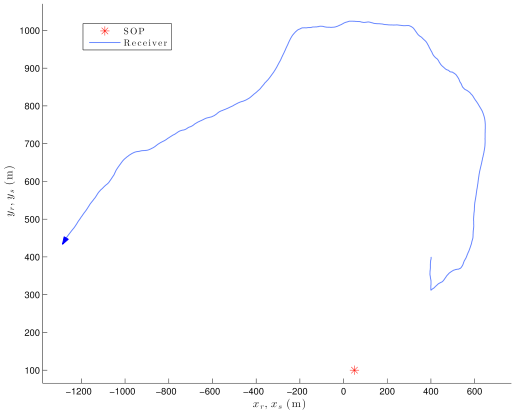

Fig. 3. Sample receiver trajectory

A.2 Results

Best OCXO Assuming the SOP's true oscillator to be a best OCXO, three sets of filters were simulated: (*i*) a matched filter; (*ii*) three mismatched, fixed filters, which assumed the SOP to have a typical OCXO, a typical TCXO, and an average clock; and (*iii*) two adaptive filters (ML and IMM). The mode probability trajectory of the IMM for a single run is illustrated in Fig. 4. The root-mean squared estimation error (RMSEE) results for the SOP's position, clock bias, and clock drift are given in Fig. 8.

Typical OCXO Assuming the SOP's true oscillator to be a typical OCXO, three sets of filters were simulated: (*i*) a matched filter; (*ii*) two mismatched, fixed filters, which assumed the SOP to have a typical TCXO and an average clock; and (*iii*) two adaptive filters. The mode probability trajectory of the IMM for a single run is illustrated in Fig. 5. The RMSEE results for the SOP's position, clock bias, and clock drift are given in Fig. 9.

Worst TCXO Assuming the SOP's true oscillator to be a worst TCXO, three sets of filters were simulated: (*i*) a matched filter; (*ii*) three mismatched, fixed filters, which assumed the SOP to have a typical OCXO, a typical TCXO, and an average clock; and (*iii*) two adaptive filters. The mode probability trajectory of the IMM for a single run is illustrated in Fig. 6. The RMSEE results for the SOP's position, clock bias, and clock drift are given in Fig. 10.

The ML and IMM adaptive filters estimates of h_0 and h_{-2} are given in Table II. The estimates from both IMM formulations (4) and (5) are reported. These ML and IMM estimates are obtained by first time-averaging (over the last 30 time steps) the estimates per simulation run, then ensemble-averaging over all simulation runs.

A.3 Discussion

The following conclusions can be drawn from the presented results. First, after a short period of transience, the mode probabilities calculated by the IMM correctly identified the true mode. However, such identification was not exact, and the performance degraded whenever the true mode coincided with the lower- or upper-bounds of $\mathbf{Q}$. Second, the estimate achieved with (5), i.e., the matrix square root, outperformed (4) in every case, except when the true $\mathbf{Q}$ was close to the upper-bound $\mathbf{Q}$ (i.e., the worst TCXO). This is consistent with the behavior reported in [39]. Third, IMM outperformed ML. Fourth, the IMM outperformed all mismatched, fixed filters, except for the case when the true SOP clock was a best OCXO and the mismatched filter was set to a fixed typical OCXO. This is due to the numerical proximity of the h parameters corresponding to a typical OCXO and the best OCXO. Fifth, the convergence of the ML filter was slow and the filter even diverged altogether in the case when the true SOP was the worst TCXO. Sixth, the adverse effects of model mismatch was demonstrated in the divergence of the filter in the case when the true SOP is the worst TCXO and the filter assumed a typical OCXO. Finally, it is worth noting that this is a difficult adaptive estimation problem, especially that the receiver's trajectory was not optimized for optimal information gathering as was discussed in [15, 19].

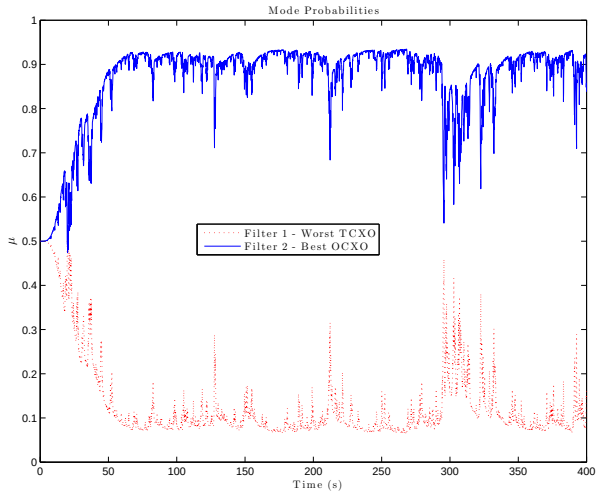

Fig. 4. Mode probability trajectory when SOP has best OCXO

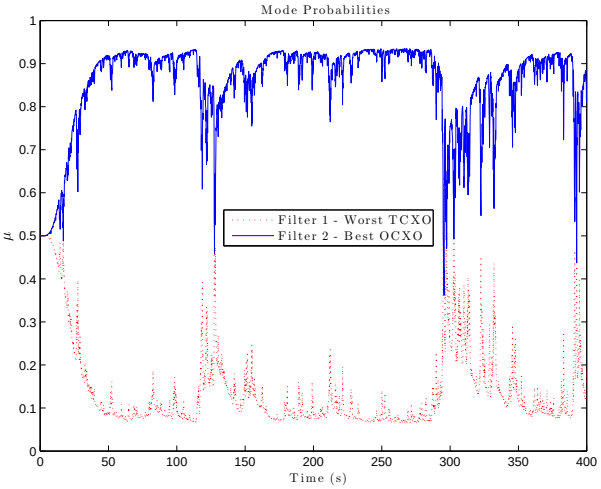

Fig. 5. Mode probability trajectory when SOP has typical OCXO

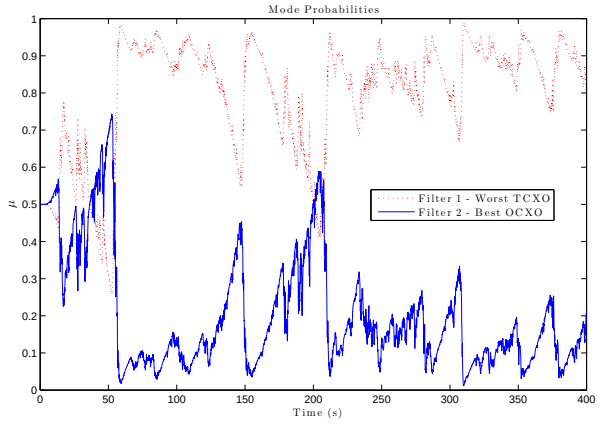

Fig. 6. Mode probability trajectory when SOP has worst TCXO

B. Multiple Receivers

This subsection demonstrates the improved estimates of the SOP's clock process noise covariance $\mathbf{Q}_{\text{clk,s}}$ (equivalently, the $h_{0,s}$ and $h_{-2,s}$ parameters) whenever multiple receivers make pseudorange observations on the same SOP and fuse such observations through a centralized adaptive filter. The same simulation settings presented in Table I were used, except for the initial position states of the five receivers, which are now randomized over different MC runs. A sample of the receivers' trajectories is shown in Fig. 7.

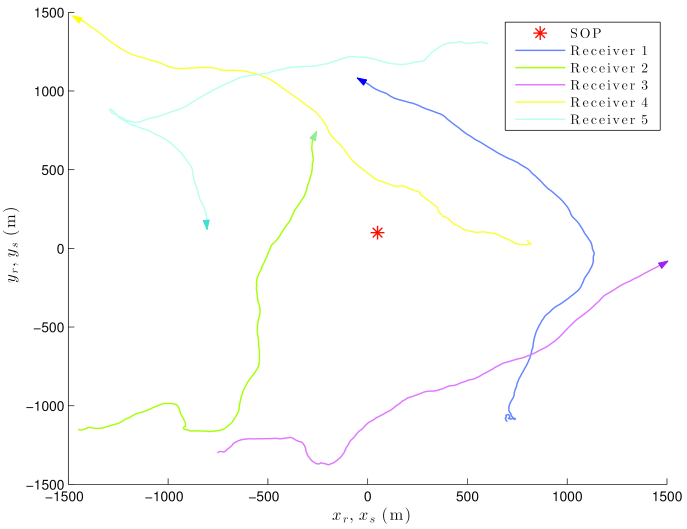

Fig. 7. Sample receivers trajectories

Similar to the single receiver case, three scenarios were considered for the truth model of the SOP: a best OCXO, a typical OCXO, and a worst TCXO. The average absolute estimation error of the h-parameters over 20 MC runs, namely $|h_{0,s} - \hat{h}_{0,s}|$ and $|h_{-2,s} - \hat{h}_{-2,s}|$, are tabulated in Tables III and IV for the IMM and ML adaptive filters, respectively. Note that the results for the ML estimating an SOP with the worst TCXO were excluded, since the filter diverged for the single receiver case.

The relative reduction in the estimation error by incorporating five receivers versus one for the ML filter was greater than that of the IMM. Nevertheless, the absolute estimation error of IMM for a fixed number of receivers was much smaller than that of the ML. Note that the estimates from the square root formulation of the IMM defined in (5) outperformed those of (4) for every case, except for the worst TCXO case, which corresponds to the case when the truth model coincided with the upper-bound of $\mathbf{Q}$.

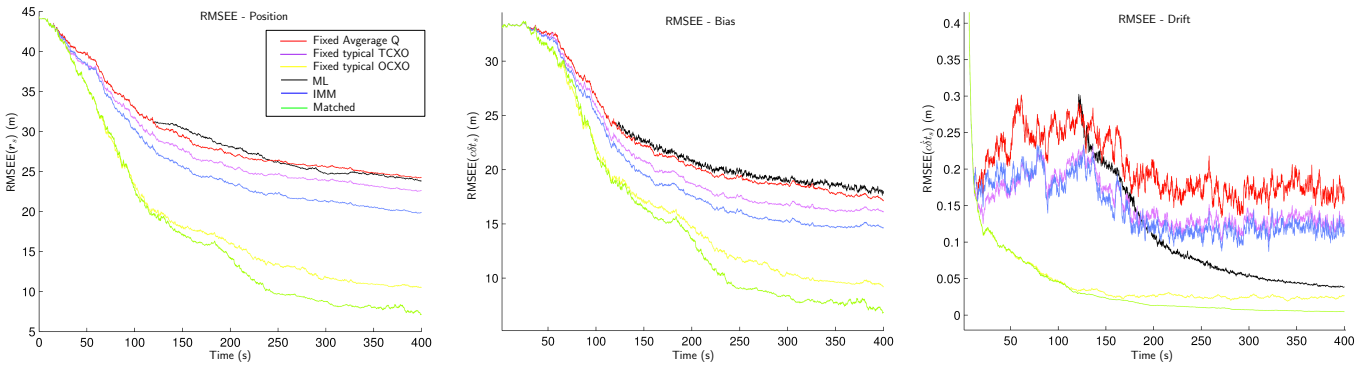

Fig. 8. RMSEE over 100 MC runs when SOP has best OCXO

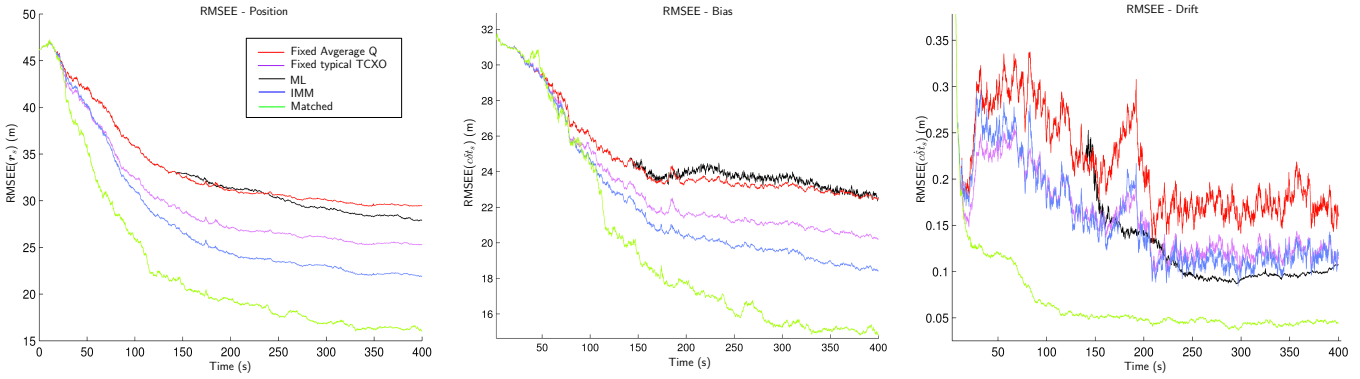

Fig. 9. RMSEE over 100 MC runs when SOP has typical OCXO

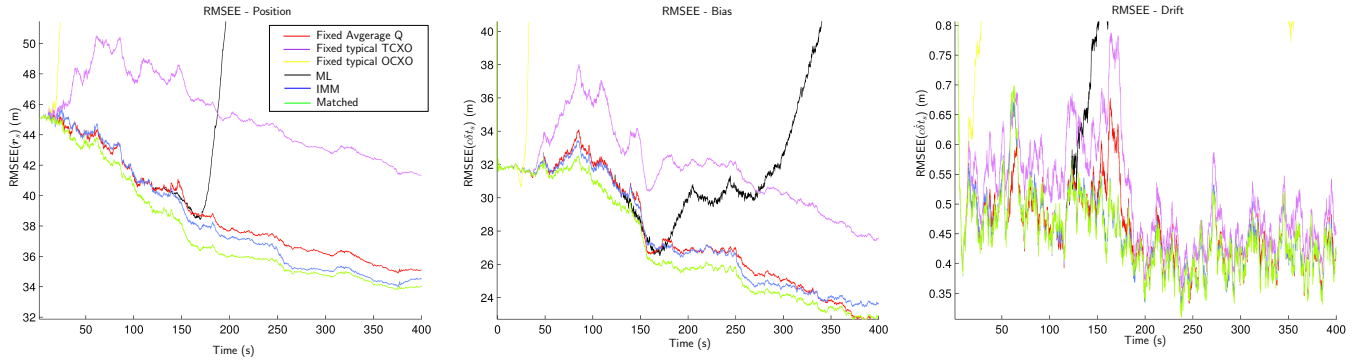

Fig. 10. RMSEE over 100 MC runs when SOP has worst TCXO

TABLE II

AVERAGE ESTIMATES OF h_0 AND h_{-2} OVER 100 MC RUNS OF ML AND IMM ADAPTIVE FILTERS

Scenario	$\boldsymbol{h_0}$	$\hat{\boldsymbol{h}}_{\mathbf{0},\mathrm{IMM}}$	$\hat{\boldsymbol{h}}_{\mathbf{0},\mathrm{IMMSD}}$	$\hat{\boldsymbol{h}}_{\mathbf{0},\mathrm{ML}}$	$\boldsymbol{h_{-2}}$	$\hat{\boldsymbol{h}}_{\mathbf{-2},\mathrm{IMM}}$	$\hat{\boldsymbol{h}}_{\mathbf{-2},\mathrm{IMMSD}}$	$\hat{\boldsymbol{h}}_{\mathbf{-2},\mathrm{ML}}$
Best OCXO	2.6×10^{-22}	5.8×10^{-21}	2.1×10^{-21}	1.0×10^{-16}	4.0×10^{-26}	5.8×10^{-21}	1.7×10^{-21}	3.6×10^{-22}
Typ. OCXO	8.0×10^{-20}	5.9×10^{-20}	2.2×10^{-20}	1.1×10^{-16}	4.0×10^{-23}	5.9×10^{-21}	1.8×10^{-21}	3.7×10^{-22}
Worst TCXO	2.0×10^{-19}	1.3×10^{-19}	0.9×10^{-19}	1.3×10^{-16}	2.0×10^{-20}	1.3×10^{-20}	0.8×10^{-20}	0.1×10^{-20}

TABLE III

AVERAGE ABSOLUTE ESTIMATION ERROR OF h_0 AND h_{-2} OF IMM OVER 20 MC RUNS FOR SINGLE AND MULTIPLE RECEIVERS

Scenario	**Estimator**	$\|h_0 - \hat{h}_0\|$ ($\times 10^{-20}$)		$\|h_{-2} - \hat{h}_{-2}\|$ ($\times 10^{-20}$)	
		One receiver	**Five receivers**	**One receiver**	**Five receivers**
Best OCXO	IMM	2.47	1.45	0.25	0.15
	IMMSD	0.54	0.26	0.04	0.02
Typical OCXO	IMM	2.48	1.35	0.25	0.14
	IMMSD	0.6	0.21	0.04	0.01
Worst TCXO	IMM	5.24	3.67	0.53	0.37
	IMMSD	7.82	5.38	0.86	0.62

TABLE IV

AVERAGE ABSOLUTE ESTIMATION ERROR OF h_0 AND h_{-2} OF ML OVER 20 MC RUNS FOR SINGLE AND MULTIPLE RECEIVERS

Scenario	$\|h_0 - \hat{h}_0\|$ ($\times 10^{-16}$)		$\|h_{-2} - \hat{h}_{-2}\|$ ($\times 10^{-20}$)	
	One receiver	**Five receivers**	**One receiver**	**Five receivers**
Best OCXO	3.05	0.12	0.370	0.07
Typical OCXO	1.36	0.01	0.23	0.05

V. EXPERIMENTAL RESULTS

A field experimental demonstration was conducted to illustrate the improvements gained from adaptive filters versus mismatched, fixed filters in estimating the states of an unknown cellular SOP. To this end, two antennas were mounted on a vehicle to acquire and track: (i) multiple Global Positioning System (GPS) signals and (ii) a signal from a nearby cellular phone tower whose signal was modulated through code division multiple access (CDMA). The GPS and cellular signals were simultaneously downmixed and synchronously sampled via two National Instruments® vector Radio Frequency Signal Analyzers (RFSAs). These front-ends fed their data to a Generalized Radionavigation Interfusion Device (GRID) software receiver [44], which simultaneously tracked all GPS L1 C/A signals in view and the signal from the cellular tower with unknown states, producing pseudorange observables for all tracked signals. Fig. 11 illustrates the hardware setup of the conducted experiment. The observables were fed into four MATLAB®-based filters:

Mismatched two mismatched, fixed filters: one assumed the SOP to be equipped with a typical OCXO, while the other assumed the SOP to be equipped with an average clock (i.e., whose process noise covariance is $\mathbf{Q}_{\text{avg}}$)
Adaptive two adaptive filters: ML and IMM

Since the states of the GPS satellite vehicles (SVs) were known, and since the receiver was tracking more than four GPS SVs throughout the experiment, the receiver's state vector $\boldsymbol{x}_r$ was fully-known. The cellular tower state vector consisted of its planar position states, clock bias, and clock drift, as defined in (1). The EKF initial state estimate $\hat{\boldsymbol{x}}(0|-1)$ was generated according to $\hat{\boldsymbol{x}}(0|-1) \sim \mathcal{N}\left[\boldsymbol{x}(0), \mathbf{P}(0|-1)\right]$, where $\boldsymbol{x}(0) \triangleq \left[\boldsymbol{r}_s^{\mathsf{T}}(0), c\delta t_s(0), 0\right]^{\mathsf{T}}$, where $\boldsymbol{r}_s^{\mathsf{T}} \triangleq [x_s(0), y_s(0)]$ is the projection of the true cellular tower location from the Earth-Centered Earth-Fixed (ECEF) coordinate frame system to a planar system, $c\delta t_s(0) = \|\boldsymbol{r}_r(0) - \hat{\boldsymbol{r}}_s(0|-1)\|_2 - \rho(0) + c\delta t_r(0)$, $\boldsymbol{r}_r^{\mathsf{T}}(0) \triangleq [x_r(0), y_r(0)]$ is the planar projection of the receiver's initial location from ECEF, and $\mathbf{P}(0|-1) = \text{diag}\left[1\times 10^3, 1\times 10^3, 3\times 10^3, 3\times 10^2\right]$ is the EKF initial estimation error covariance matrix. Fig. 12 shows the receiver traversed trajectory during the collection of the pseudorange observations, the true and estimated location of the cellular phone tower by the four filters, and the associated 2σ uncertainty ellipse produced by each filter's estimation error covariance. Fig. 13 shows the mode probability trajectory for the IMM filter. Note that after a short period of transience, the mode probabilities identified the cellular CDMA oscillator to have around 70% best OCXO value and 30% worst TCXO value. Note that while the cellular tower was within the estimation uncertainty ellipses of all filter, the cellular tower position estimates from the two adaptive filters were closer to the true tower location than the estimates produced by the fixed, mismatched filters. This performance was consistent among multiple MC runs with randomized initial estimates $\hat{\boldsymbol{x}}(0|-1)$. Table V presents the average absolute distance error between the true tower location and the estimated tower location, i.e.

$|\boldsymbol{r}_s - \hat{\boldsymbol{r}}_s|$, over 10 MC runs. It is noted that the IMM outperformed the ML adaptive filter. Moreover, these results along with the mode probability trajectories suggest that the cellular oscillator is less stable than a typical OCXO, but more stable than an average clock. Table VI presents the average estimated h_0 and h_{-2} parameters by the ML and IMM filters over 10 MC runs.

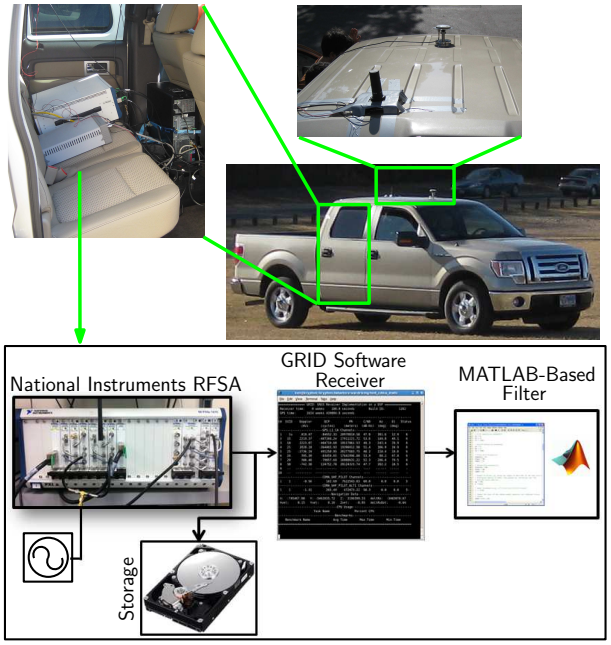

Fig. 11. Experiment hardware setup

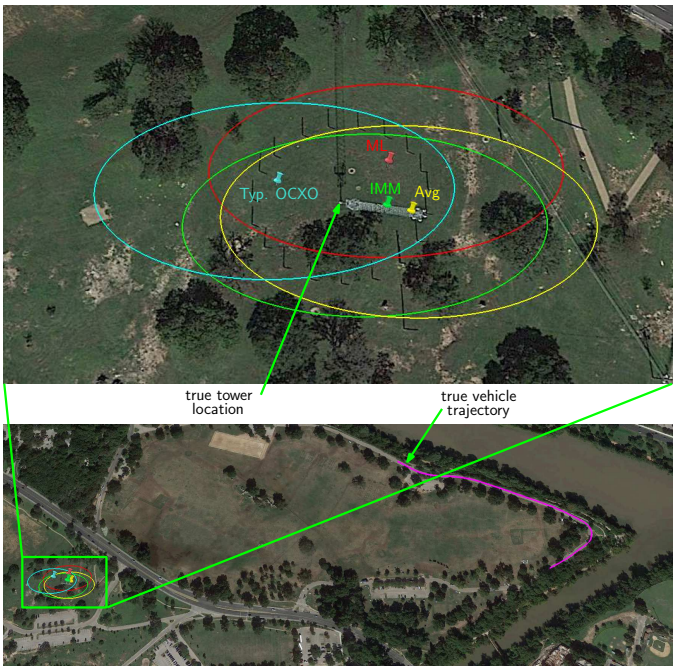

Fig. 12. Receiver traversed trajectory, true cellular tower location, estimated tower location with fixed filters that assumed a typical OCXO and an average clock, estimated tower location with ML and IMM adaptive filters, and associated estimation error ellipses

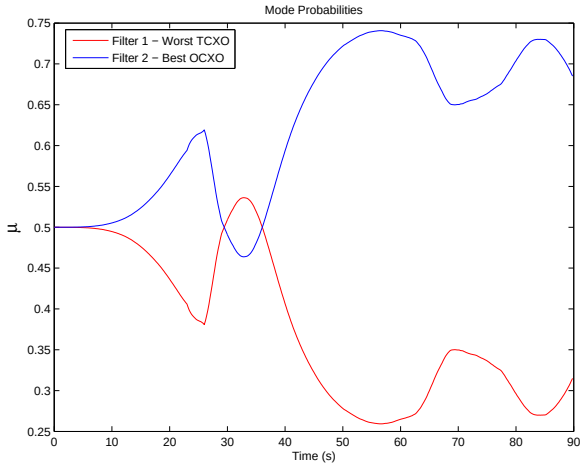

Fig. 13. Mode probabilities of IMM filter

TABLE V
AVERAGE ABSOLUTE DISTANCE ERROR BETWEEN TRUE TOWER LOCATION AND ESTIMATED TOWER LOCATION

Filter	$\lvert\boldsymbol{r}_s - \hat{\boldsymbol{r}}_s\rvert$ **(m)**
Typical OCXO	28.06
Average clock	21.66
ML	20.82
IMM	20.04

TABLE VI
CELLULAR CDMA TOWER OSCILLATOR h_0 AND h_{-2} ESTIMATES

Adaptive Filter	$\hat{\boldsymbol{h}}_{\boldsymbol{0}}$	$\hat{\boldsymbol{h}}_{\boldsymbol{-2}}$
ML	4.3×10^{-19}	2.7×10^{-22}
IMM	3.6×10^{-20}	7.0×10^{-21}

VI. CONCLUSIONS

This paper studied the problem of adaptive estimation of unknown SOPs. To exploit unknown SOPs for positioning and navigation, the receiver must not only estimate the states of such SOPs, but also must estimate a set of parameters that characterize the stability of the SOPs' oscillators. This necessitates the development of adaptive filters. Two candidate adaptive filters were studied: a simple ML innovation-based filter and a more involved IMM filter. Numerical and experimental results demonstrated the superiority of IMM over ML. Moreover, numerical simulation results demonstrated the adverse effects of model mismatch in fixed filters in that a fixed, mismatched filter may diverge altogether.

References

[1] Z. Kassas, "Collaborative opportunistic navigation," *IEEE Aerospace and Electronic Systems Magazine*, vol. 28, no. 6, pp. 38–41, Jun. 2013.

[2] ——, "Analysis and synthesis of collaborative opportunistic navigation systems," Ph.D. dissertation, The University of Texas at Austin, USA, 2014.

[3] C. Yang, T. Nguyen, and E. Blasch, "Mobile positioning via fusion of mixed signals of opportunity," *IEEE Aerospace and Electronic Systems Magazine*, vol. 29, no. 4, pp. 34–46, Apr. 2014.

[4] C. Yang, T. Nguyen, E. Blasch, and D. Qiu, "Assessing terrestrial wireless communications and broadcast signals as signals of opportunity for positioning and navigation," in *Proc. of ION GNSS*, Sep. 2012, pp. 3814–3824.

[5] K. Pesyna, Z. Kassas, J. Bhatti, and T. Humphreys, "Tightly-coupled opportunistic navigation for deep urban and indoor positioning," in *Proc. of ION GNSS*, Sep. 2011, pp. 3605–3617.

[6] P. Thevenon, S. Damien, O. Julien, C. Macabiau, M. Bousquet, L. Ries, and S. Corazza, "Positioning using mobile TV based on the DVB-SH standard," *NAVIGATION, Journal of the Institute of Navigation*, vol. 58, no. 2, pp. 71–90, 2011.

[7] J. McEllroy, "Navigation using signals of opportunity in the AM transmission band," Master's thesis, Air Force Institute of Technology, Wright-Patterson Air Force Base, Ohio, USA, 2006.

[8] L. Bruno and P. Robertson, "WiSLAM: improving FootSLAM with WiFi," in *Proc. of International Conference on Indoor Positioning and Indoor Navigation*, Sep. 2011, pp. 1–10.

[9] M. Joerger, L. Gratton, B. Pervan, and C. Cohen, "Analysis of Iridium-augmented GPS for floating carrier phase positioning," *NAVIGATION, Journal of the Institute of Navigation*, vol. 57, no. 2, pp. 137–160, 2010.

[10] K. Pesyna, Z. Kassas, and T. Humphreys, "Constructing a continuous phase time history from TDMA signals for opportunistic navigation," in *Proc. of IEEE/ION Position Location and Navigation Symposium*, Apr. 2012, pp. 1209–1220.

[11] L.-P. Gill, D. Grenier, and J.-Y. Chouinard, "Use of XM radio satellite signal as a source of opportunity for passive coherent location," *IET Radar, Sonar, & Navigation*, vol. 5, no. 5, pp. 536–544, Jun. 2011.

[12] D. Zheng, G. Chen, and J. Farrell, "Navigation using linear photo detector arrays," in *Proc. of IEEE International Conference on Control Applications*, Aug. 2013, pp. 533–538.

[13] Z. Kassas and T. Humphreys, "Observability analysis of collaborative opportunistic navigation with pseudorange measurements," *IEEE Trans. on Intelligent Transportation Systems*, vol. 15, no. 1, pp. 260–273, Feb. 2014.

[14] ——, "Observability and estimability of collaborative opportunistic navigation with pseudorange measurements," in *Proc. of ION GNSS*, Sep. 2012, pp. 621–630.

[15] ——, "Motion planning for optimal information gathering in opportunistic navigation systems," in *Proc. of AIAA Guidance, Navigation, and Control Conference*, Aug. 2013, pp. 4551–4565.

[16] Z. Kassas, J. Bhatti, and T. Humphreys, "Receding horizon trajectory optimization for simultaneous signal landscape mapping and receiver localization," in *Proc. of ION GNSS*, Sep. 2013, pp. 1962–1969.

[17] Z. Kassas and T. Humphreys, "Receding horizon trajectory optimization in opportunistic navigation environments," *IEEE Trans. on Aerospace and Electronic Systems*, 2014, accepted.

[18] ——, "The price of anarchy in active signal landscape map building," in *Proc. of IEEE Global Conference on Signal and Information Processing*, Dec. 2013, pp. 165–168.

[19] ——, "Greedy motion planning for simultaneous signal landscape mapping and receiver localization," *IEEE Journal on Selected Topics in Signal Processing*, 2014, under review.

[20] A. Mohamed and K. Schwarz, "Adaptive Kalman filtering for INS/GPS," *Journal of Geodesy*, vol. 73, no. 4, pp. 193–203, 1999.

[21] C. Hide, T. Moore, and M. Smith, "Adaptive Kalman filtering algorithms for integrating GPS and low cost INS," in *Proc. of IEEE/ION Position Location and Navigation Symposium*, Apr. 2004, pp. 227–233.

[22] W. Ding, J. Wang, C. Rizos, and D. Kinlyside, "Improving adaptive Kalman estimation in GPS/INS integration," *The Journal of Navigation*, vol. 60, no. 3, pp. 517–529, Sep. 2007.

[23] M. Yu, "INS/GPS integration system using adaptive filter for estimating measurement noise variance," *IEEE Trans. on Aerospace and Electronic Systems*, vol. 48, no. 2, pp. 1786–1792, Apr. 2012.

[24] P. Misra and P. Enge, *Global Positioning System: Signals, Measurements, and Performance*, 2nd ed. Ganga-Jamuna Press, 2010.

[25] N. Kasdin, "Discrete simulation of colored noise and stochastic processes and $1/f^{\alpha}$ power law noise generation," *Proc. of the IEEE*, vol. 83, no. 5, pp. 802–827, May 1995.

[26] J. Timmer and M. Koenig, "On generating power law noise," *Astronomy and Astrophysics*, vol. 300, pp. 707–710, 1995.

[27] J. Barnes, A. Chi, R. Andrew, L. Cutler, D. Healey, D. Leeson, T. McGunigal, J. Mullen, W. Smith, R. Sydnor, R. Vessot, and G. Winkler, "Characterization of frequency stability," *IEEE Trans. on Instrumentation and Measurement*, vol. 20, no. 2, pp. 105–120, May 1971.

[28] A. Thompson, J. Moran, and G. Swenson, *Interferometry and Synthesis in Radio Astronomy*, 2nd ed. John Wiley & Sons, 2001.

[29] Y. Bar-Shalom, X. Li, and T. Kirubarajan, *Estimation with Applications to Tracking and Navigation*. New York, NY: John Wiley & Sons, 2002.

[30] R. Brown and P. Hwang, *Introduction to Random Signals and Applied Kalman Filtering*, 3rd ed. John Wiley & Sons, 2002.

[31] R. Mehra, "Approaches to adaptive filtering," *IEEE Trans. on Automatic Control*, vol. 17, no. 5, pp. 693–698, Oct. 1972.

[32] S. Sarkka and A. Nummenmaa, "Recursive noise adaptive Kalman filtering by variational bayesian approximations," *IEEE Trans. on Automatic Control*, vol. 3, no. 4, pp. 596–600, Mar. 2009.

[33] Y. Yang and W. Gao, "A Bayesian solution to the problem of state estimation in an unknown noise environments," *Journal of Geodesy*, vol. 80, no. 4, pp. 177–183, 2006.

[34] R. Reynolds, "Robust estimation of covariance matrices," *IEEE Trans. on Automatic Control*, vol. 35, no. 9, pp. 1047–1051, Sep. 1990.

[35] B. Friedland, "Estimating noise variances by using multiple observers," *IEEE Trans. on Aerospace and Electronic Systems*, vol. 18, no. 4, pp. 442–448, Jul. 1982.

[36] Y. Bar-Shalom, "Optimal simultaneous state estimation and parameter identification in linear discrete-time systems," *IEEE Trans. on Automatic Control*, vol. 17, no. 3, pp. 308–319, Jun. 1972.

[37] J. Burg, D. Luenberger, and D. Wenger, "Estimation of structured covariance matrices," *Proc. of the IEEE*, vol. 70, no. 9, pp. 963–974, Sep. 1982.

[38] P. Maybeck and P. Hanlon, "Multiple-model adaptive estimation using a residual correlation Kalman filter bank," *IEEE Trans. on Aerospace and Electronic Systems*, vol. 36, no. 2, pp. 393–406, Apr. 2000.

[39] R. Li, X., and Y. Bar-Shalom, "A recursive multiple model approach to noise identification," *IEEE Trans. on Aerospace and Electronic Systems*, vol. 30, no. 3, pp. 671–684, Jul. 1994.

[40] R. Mehra, "On the identification of variances and adaptive Kalman filtering," *IEEE Trans. on Automatic Control*, vol. 15, no. 2, pp. 175–184, Apr. 1970.

[41] A. Mohamed, "Optimizing the estimation procedure in INS/GPS integration for kinematic applications," Ph.D. dissertation, University of Calgary, Canada, 1999.

[42] H. Blom and Y. Bar-Shalom, "The interacting multiple model algorithm for systems with Markovian switching coefficients," *IEEE Trans. on Automatic Control*, vol. 33, no. 8, pp. 780–783, Aug. 1988.

[43] J. Curran, G. Lachapelle, and C. Murphy, "Digital gnss pll design conditioned on thermal and oscillator phase noise," *IEEE Trans. on Aerospace and Electronic Systems*, vol. 48, no. 1, pp. 180–196, Jan. 2012.

[44] T. Humphreys, J. Bhatti, T. Pany, B. Ledvina, and B. O'Hanlon, "Exploiting multicore technology in software-defined GNSS receivers," in *Proc. of ION GNSS*, Sep. 2009, pp. 326–338.